

7.4  $E\alpha$ , and for the cylinder with a 60° conical end it is estimated as  $\sigma_{\max} = 10.4 E\alpha$ . Although the meniscus profile is not the same in all the castings, the maximum stress at the meniscus end is often smaller than that at the conical corners and is estimated as  $\sigma = 4.6 E\alpha$ .

As an aid to rocket grain designers these stress values are compared with a number of other plane-stress, plane-strain, and axisymmetric solutions in a table at the end of the paper. The other solutions are for the same load, restrained shrinkage, and for various geometries.

## Stresses in Hollow Cylinders with Conical Ends Bonded to Shell and Shrunk

A. J. DURELLI,\* V. J. PARKS,† AND K. CHANDRASHEKHARA‡  
The Catholic University of America, Washington, D. C.

This paper deals with the three-dimensional photoelastic analysis of stresses and strains in two long, hollow circular cylinders with conical ends of 45° and 60°. The cylinders were bonded to a steel casing on the outer surface. The stresses and strains due to restrained shrinkage have been determined at the interface. The maximum stress for both geometries was found to occur at the end of the bond, and to be about 40% higher in the 60° cylinder than in the 45° cylinder. A study was also made at the opposite end of the two cylinders, where a natural meniscus was formed. The results should be of interest in the design of solid-propellant rocket grains.

### Introduction

PREVIOUS papers have reported results of an extensive study on stresses and strains in rectangular strips and plates, bonded on one face and shrunk<sup>1</sup> or subjected to biaxial restrained shrinkage,<sup>2</sup> and a study on the stresses in a square slab bonded on one face to a rigid plate and shrunk, which simulates a plane strain condition.<sup>3,4</sup> Cylinders with toroidal cavities also have been tested, and the results are reported elsewhere.<sup>5</sup> This paper is concerned with three-dimensional photoelasticity studies of the stresses and strains in two hollow circular cylinders having two different conical ends (at angles of 45° and 60°, respectively, with the bonded surface) and subjected to restrained shrinkage. As the shell is assumed to be rigid, the restrained shrinkage load can be considered as a uniform strain applied in the tangential direction on the bonded surface of the cylinder and a uniform displacement normal to the bonded surface. The uniform strain is specified as  $\alpha$  and is equal to the difference between the free shrinkages of the propellant and of the shell. The uniform displacement will be  $\alpha r$  when  $r$  is the radius of the bonded surface.

In the frozen stress technique that was used, thin slices were removed from the frozen stress model for analysis. The isochromatic patterns obtained give the maximum shear stress at any point in the slice and the maximum principal stress on free boundaries. The determination of the principal stresses and strains in the interior of the body and on the bonded surface requires further analysis. In this study the stress and strain distribution was obtained only along the bonded interface surface which is of particular interest as a

region where failure is likely to occur. This type of failure at the interface is commonly referred to as bond failure, as opposed to the material failure which may occur in the interior of the body or on a free surface.

Each of the hollow circular cylinders used in this study (Fig. 1) was cast directly in a steel shell using the epoxy formula suggested by Sampson,<sup>6</sup> 2 parts-by-weight (pbw) of Bakelite resin ERL-2274, 2 pbw of Bakelite resin ERL-2795, and one pbw Bakelite hardener ZYL-0803. The two resins were heated to 180°F in separate containers, then mixed and deaerated for 20 min at 27 in. Hg vacuum. The mixture was then cooled to 90°F, and the hardener was added slowly and mixed thoroughly for ~10 min. The epoxy was poured into the steel molds and was allowed to set for 24 hr. Then the complete system was placed in the oven and was heated to 170°F at the rate of 5°F/hr. The epoxy and the mold were cooled to room temperature at 2°F/hr. A free disk and a ring shrunk on a plug were also cast at the same time for calibration.

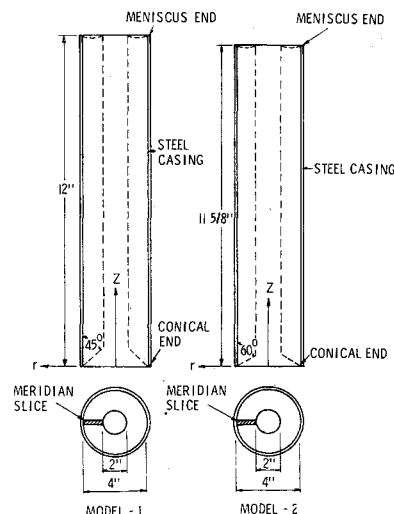


Fig. 1 Geometry and dimensions of hollow circular cylinders.

Received November 3, 1969; revision received May 12, 1970.

\* Professor, Civil Engineering and Mechanics Department.

† Associate Professor, Civil Engineering and Mechanics Department.

‡ Postdoctoral Fellow, Civil Engineering and Mechanics Department; now Assistant Professor, Indian Institute of Science, Bangalore, India.

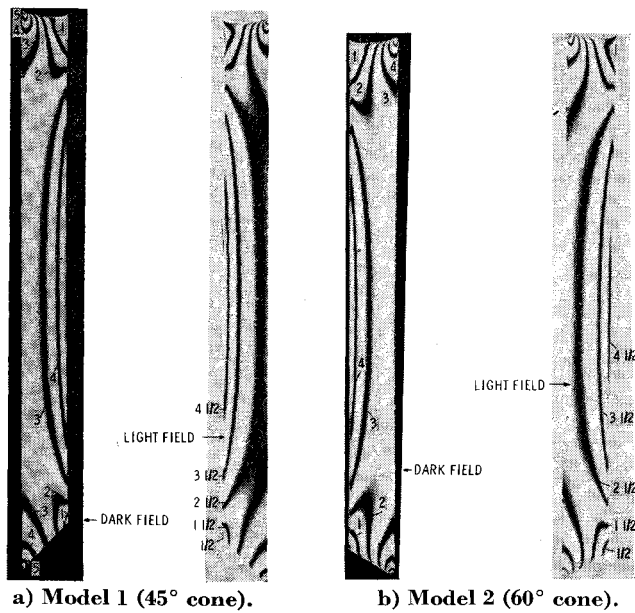


Fig. 2 Isochromatic patterns of the meridian slices of the cylinders with cones ( $t = \frac{1}{8}$  in.).

### Analysis

The normalized stress concentration factor  $K$  is defined as

$$K = \sigma_{\max}/E\alpha = 2(\tau_{\max})_{\max}/E\alpha \quad (1)$$

where  $(\tau_{\max})_{\max}$  is the maximum shear stress at a point on a free boundary, where the maximum shear stress is the highest;  $\tau_{\max}$  is the maximum shear stress at a point;  $E$  is the Young's modulus; and  $\alpha$  is the differential shrinkage between grain and shell.

The stress-optic law is given by

$$\tau_{\max} = (\sigma_1 - \sigma_2)/2 = nf_\sigma/t = nF_\sigma \quad (2)$$

where  $\sigma_1$  and  $\sigma_2$  are the principal stresses;  $n$  is the fringe order;  $f_\sigma$  is the material stress fringe value;  $t$  is the thickness of the slice; and  $F_\sigma$  is the model fringe value for a given thickness  $t$ . By means of Eq. (2), the expression for  $K$  can be written as

$$K = 2n_{\max}F_\sigma/E\alpha \quad (3)$$

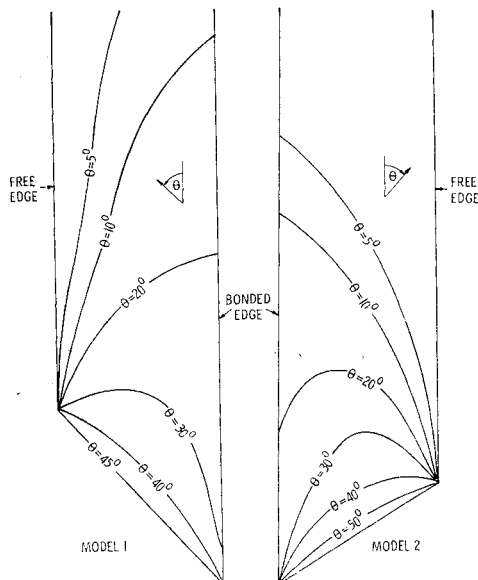


Fig. 3 Isoclinic patterns in models 1 and 2.

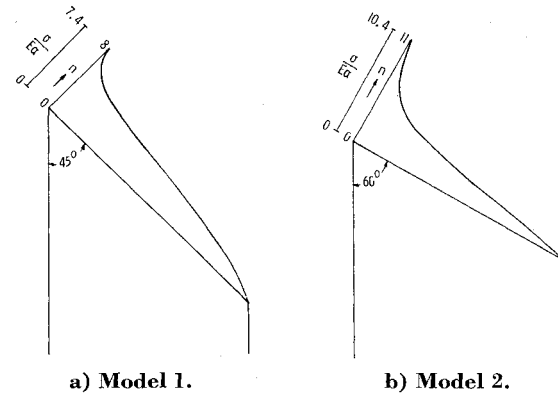


Fig. 4 Normalized stresses on the inclined edges ( $45^\circ$  or  $60^\circ$ ) of the meridian slices of the cylinders ( $t = \frac{1}{8}$  in.).

where  $n_{\max}$  is the maximum fringe order on the free boundary of the slice.

The model fringe value  $F_\sigma$  can be determined in terms of  $E\alpha$ , assuming that the central part of the hollow circular cylinder is in a state of plane strain. For a sufficiently long cylinder restrained on the outer surface and subjected to shrinkage, the difference in principal stresses at sections far from the end can be determined from Lamé's solution as

$$\sigma_z - \sigma_r = \frac{E\alpha a^2}{1 - 2\nu + (a/b)^2} \left( \frac{1}{r^2} + \frac{1}{b^2} \right) \quad (4)$$

where  $\sigma_z$  and  $\sigma_r$  are the axial and radial stresses;  $r$  is the radius of the point of interest;  $a$  and  $b$  are the inner and outer radii of the cylinder; and  $\nu$  is Poisson's ratio.

The stress-optic law for the meridian slice can be written as

$$\frac{1}{2}(\sigma_z - \sigma_r) = nF_\sigma \quad (5)$$

Using Eqs. (4) and (5),  $F_\sigma$  can be determined from

$$F_\sigma = \frac{E\alpha a^2}{1 - 2\nu + (a/b)^2 n^*} \left( \frac{1}{r^2} + \frac{1}{b^2} \right) \quad (6)$$

where  $n^*$  is the fringe order in the meridian slice at a point situated at a distant  $r$  from the center. Using Eq. (6) and assuming  $\nu = 0.5$ ,

$$F_\sigma = (E\alpha/n^*)(b^2/r^2 + 1) \quad (7)$$

The Cartesian shear stress  $\tau_{rz}$  is

$$\tau_{rz} = \tau_{\max} \sin 2\theta = nF_\sigma \sin 2\theta \quad (8)$$

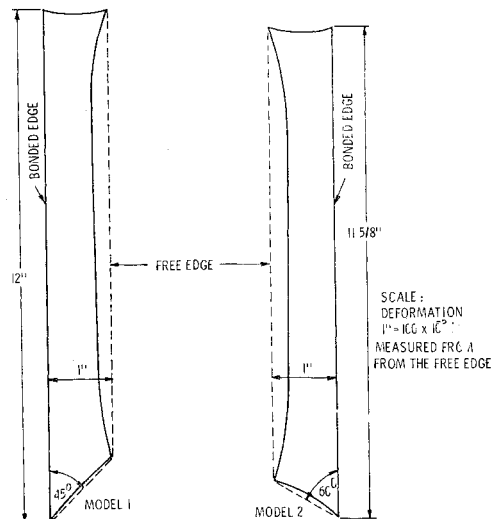


Fig. 5 Deformation of the inner boundary due to restrained shrinkage.

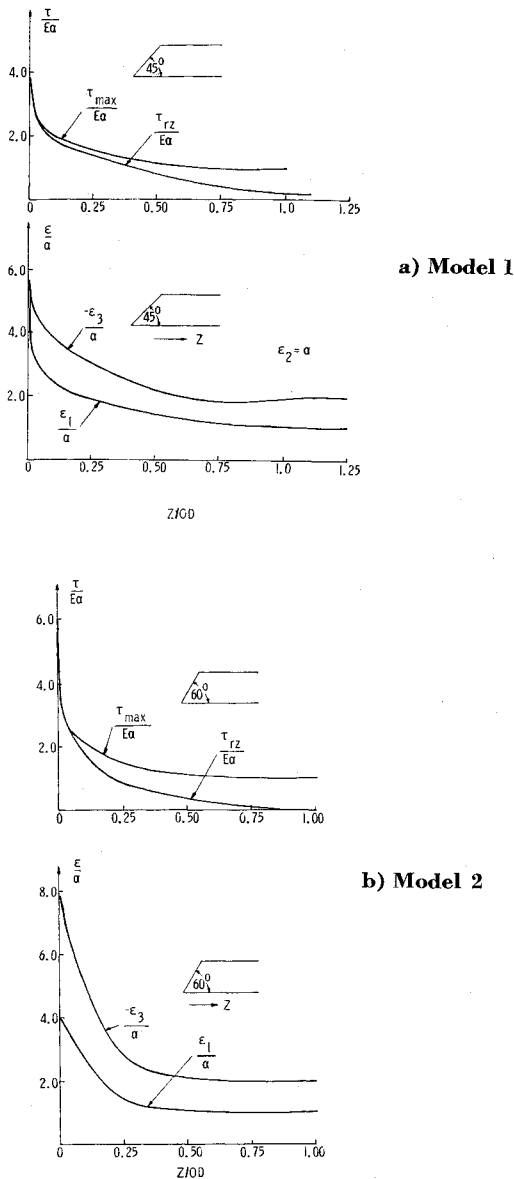


Fig. 6 Shear stresses and principal strain distributions along the interfaces.

where  $\Theta$  is the angle measured counter-clockwise from the horizontal axis to the  $\sigma_1$  direction (isoclinic parameter).

The principal strains  $\epsilon_1$ ,  $\epsilon_2$ , and  $\epsilon_3$  at the interface of the meridian slice can be obtained from the principal stresses using Hooke's law. However, equations to determine the principal strains can be derived directly using the photoelasticity and Mohr's circle.

The strain-optic law is

$$\epsilon_1 - \epsilon_3 = 2nF_\epsilon \quad (9)$$

where  $F_\epsilon$  is the model strain fringe value for a given thickness  $t$ . From Mohr's circle it can be shown that

$$\epsilon_1 = \epsilon_t + [(\epsilon_1 - \epsilon_3)/2](1 - \cos 2\Theta) \quad (10)$$

$$\epsilon_3 = \epsilon_t - [(\epsilon_1 - \epsilon_3)/2](1 + \cos 2\Theta) \quad (11)$$

where  $\epsilon_t$  is the tangential strain at the interface. Substituting (9) into (10) and (11) and letting  $\epsilon_t = \alpha$ ,

$$\epsilon_1 = \alpha + nF_\epsilon(1 - \cos 2\Theta) \quad (12)$$

$$\epsilon_3 = \alpha - nF_\epsilon(1 + \cos 2\Theta) \quad (13)$$

If these principal strains are normalized with respect to the

differential shrinkage  $\alpha$ , Eqs. (12) and (13) can be written as

$$(\epsilon_1/\alpha) = 1 + (nF_\epsilon/\alpha)(1 - \cos 2\Theta) \quad (14)$$

$$(\epsilon_3/\alpha) = 1 - (nF_\epsilon/\alpha)(1 + \cos 2\Theta) \quad (15)$$

The other principal strain which is normal to the plane of meridian slice (circumferential strain) is known to be equal to the tangential strain at the interface, i.e.,

$$\epsilon_z = \alpha, \text{ or } \epsilon_z/\alpha = 1 \quad (16)$$

To compute the normalized principal strains from Eq. (14), the factor  $(F_\epsilon/\alpha)$  should be known. The relationship between model strain fringe value  $F_\epsilon$  and the model stress fringe value  $F_\sigma$  is given by

$$F_\sigma = F_\epsilon[E/(1 + \nu)] \quad (17)$$

Substituting this expression into Eq. (7) gives

$$\frac{F_\epsilon}{\alpha} = \left( \frac{1 + \nu}{n^*} \right) \left( \frac{b^2}{r^2} + 1 \right) \quad (18)$$

For the present case, for  $\nu = 0.5$  and  $t = 0.125$  in., it was found that

$$F_\epsilon/\alpha = 0.69 \text{ (model 1)} \quad (19)$$

$$F_\epsilon/\alpha = 0.72 \text{ (model 2)} \quad (20)$$

Since the stresses and strains were normalized, it was not necessary to use the value of  $\alpha$ . However,  $\alpha$  was estimated by measuring the free shrinkage on a specimen of the cured epoxy and was 0.00803 in that test. For general information,  $F_\epsilon$  can be estimated as  $F_\epsilon = 0.00585$  in./in./fringe for  $t = 0.125$  in.

## Results

The isochromatic patterns obtained from the meridian slices of the two models having conical ends of  $45^\circ$  and  $60^\circ$  are shown in Figs. 2a and 2b, respectively. The isoclinics near the corner for both models are shown in Fig. 3. Plots of fringe orders along the inclined edges of the meridian slices for the two models are shown in Fig. 4. The stress concentration factors as defined by Eq. (1) are also indicated. Figure 5 shows the deformation of the inner boundary, due to the restrained shrinkage; for the two models. The normalized maximum shear stresses, cartesian shear stresses, and principal strain distributions along the interfaces and on the conical end sides for the two models are shown in Fig. 6. The distribution of maximum shear stress, cartesian shear

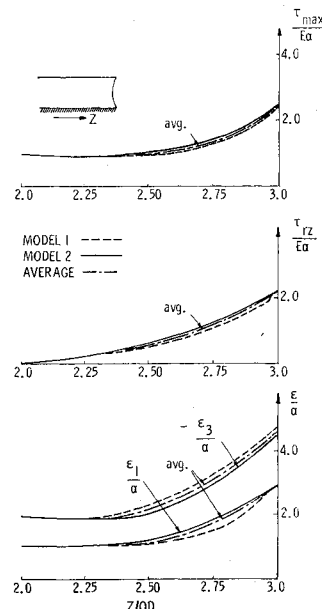


Fig. 7 Shear stresses and principal strain distributions along the interface in the cylinders with meniscus ends (average of two models).

stress and principal strains along the interface on the meniscus end side are shown in Fig. 7, which is the average of two models.

### Considerations on Analysis of the Corner

The corner at the intersection of the bonded and free surfaces is particularly difficult to analyze. The free surface requires that the normal and shear stresses on that surface be zero. It is assumed that on the bonded edge, the tangential strain is equal to the difference of thermal contraction of the two materials ( $\epsilon_t = \alpha$ ).

At the corner these two conditions lead to different results. For example, applying the free boundary conditions, the strain  $\epsilon_1/\alpha$  would be computed as

$$\epsilon_1/\alpha - \epsilon_3/\alpha = 2\nu F_e/\alpha \quad (21)$$

with

$$\epsilon_3/\alpha = -\nu\epsilon_1/\alpha \quad (22)$$

$$\epsilon_1/\alpha = 2\nu F_e/(1 + \nu)\alpha \quad (23)$$

$$\epsilon_3/\alpha = -2\nu F_e/(1 + \nu)\alpha \quad (24)$$

for  $\nu = \frac{1}{2}$

$$\epsilon_1/\alpha = (\frac{4}{3})\nu F_e/\alpha \quad (25)$$

$$\epsilon_3/\alpha = -(\frac{2}{3})\nu F_e/\alpha \quad (26)$$

Comparison of Eqs. (14) and (15) with (25) and (26) shows that depending on the isoclinic angle shown in Fig. 2b, differ-

ent results will be obtained near the corner on the free and bonded boundaries. Thus, the results in Fig. 6 should be considered as applying near the corner on the respective boundaries, but not at the corner point.

The foregoing reservations are of a theoretical nature. Although the comparison was made in terms of fringes, the difficulty would occur regardless of the value of measured fringes. Beside there are still experimental difficulties. The optical and photographic techniques do not permit a resolution higher than  $\sim 0.001$  in. Thus, both the photoelastic pattern and the geometry within 0.001 in. of the corner are in doubt. The corner may have a radius smaller than 0.001 in. Fringes within 0.001 in. of the corner may be undetected. Very near the corner, the boundary condition  $\epsilon_{\tan} = \alpha$  may not be satisfied. All of these difficulties must be taken into account at the corner point in considering the results reported here.

### Discussion

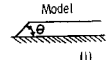
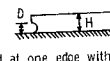
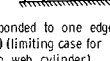
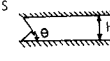
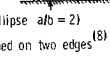
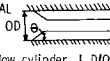

The highest stress, in both the models, occurs at the corner of the conical end. The highest stress determined on the bonded surface for the cylinder with a  $45^\circ$  conical end is  $\sigma = 7.4E\alpha$ , and for cylinder with a  $60^\circ$  conical end, we estimate that  $\sigma = 10.4E\alpha$ . Table 1 compares the stress concentration factors at the ends of bonded plates and cylinders with the results for other cases taken from previously published results.

Some investigation regarding the maximum stress at the meniscus end was also made. It was found, from a number of model castings, that the meniscus profile is not the same in all the castings. However, the results obtained here indicated that the maximum stress at the meniscus end tends to be less than that of the sharp corners. The maximum stress at the meniscus end was estimated as  $\sigma = 4.6E\alpha$ .

### References

- 1 Parks, V. J., Chiang, F.-P., and Durelli, A. J., "Maximum Stress at the Angular Corners of Long Strips Bonded on One Side and Shrunk," *Experimental Mechanics*, Vol. 8, No. 6, 1968, pp. 278-281.
- 2 Durelli, A. J., Parks, V. J., and Bhadra, P., "Experimental Determination of Stresses and Strains in a Rectangular Plate Subjected to Biaxial Restrained Shrinkage," *British Journal Applied Physics*, Vol. 17, 1966, pp. 917-926.
- 3 Durelli, A. J., Parks, V. J., and del Rio, C. J., "Stresses in a Square Slab Bonded on One Face to a Rigid Plate and Shrunk," *Acta Mechanica*, Vol. 3, No. 4, 1967, pp. 352-359.
- 4 Durelli, A. J., Parks, V. J., and del Rio, C. J., "Stresses in Square Slabs with Different Edge Geometries When Bonded on One Face to a Rigid Plate and Shrunk," *Experimental Mechanics*, Vol. 7, No. 11, 1967, pp. 481-484.
- 5 Durelli, A. J., Parks, V. J., and del Rio, C. J., "Stresses, Strains and Displacements Associated with the Restrained Shrinkage of Cylinders with Toroidal Cavities," *Recent Advances in Engineering Science*, edited by C. Eringen, Vol. 3, 1968.
- 6 Sampson, R. C., "A Three-Dimensional Photoelastic Method for Analysis of Differential Contraction Stresses," *Experimental Mechanics*, Vol. 3, No. 10, 1963, pp. 225-236.
- 7 Durelli, A. J. and Parks, V. J., "Photoelastic Stress Analysis on the Bonded Interface of a Strip with Different End Configurations," *The American Ceramic Society Bulletin*, Vol. 46, No. 6, 1967, pp. 582-586.
- 8 Durelli, A. J., Parks, V. J., and Lee, H.-C., "Stress Concentrations around Elliptical Perforations in Shrunk Plates with Bonded Boundaries," *Journal of Spacecraft and Rockets*, Vol. 5, No. 12, Dec. 1968, pp. 1499-1501.

**Table 1 Maximum stress at the end of bonded plates and cylinders subjected to restrained shrinkage**

2-DIMENSIONAL PLANE STRESS		Angles	Circles	Ellipses	K max(t)	$\nu/E\alpha$
	Boned at one edge (1)	$\theta = 45^\circ$	---	---	---	3.75
		$\theta = 90^\circ$	---	---	---	7.13
		$\theta = 135^\circ$	---	---	---	6.25
	Boned at one edge with semicircular cut outs(7)		$D/H = 1/8$	---	---	1.2
			$D/H = 2$	---	---	0.78
2-DIMENSIONAL PLANE STRAIN						
	Slab bonded to one edge, (3); (4) (limiting case for a thin web cylinder)	$\theta = 45^\circ$	---	---	---	1.9
		$\theta = 90^\circ$	---	---	---	3.0
		$\theta = 135^\circ$	---	---	---	3.3
			Inward	---	---	1.7
			outward	---	---	3.4
2-DIMENSIONAL PLANE STRESS						
	Boned on two edges (8)	$\theta = 45^\circ$	---	---	---	1.7
		$\theta = 60^\circ$	---	---	---	2.3
	(Ellipse $a/b = 2$ )		$D/H = 0.02$	---	---	5.6
			$D/H = 1$	---	---	1.4
			$a/H = 0.1^*$	---	---	5.4
			$a/H = 0.1^{**}$	---	---	4.0
			$a/H = 1$	---	---	1.9
3-DIMENSIONAL						
	Hollow cylinder 1, $D/O, D = 0.5$	$\theta = 45^\circ$	---	---	---	3.7
		$\theta = 60^\circ$	---	---	---	5.2
	Hollow cylinder with toroidal cavity (5)	1, $D/O, D = 0.37$	---	$A/O D - 1 D = 0.25$	---	6.6
		1, $D/O, D = 0.42$	---	$A/O D - 1 D = 0.33$	---	6.4

\*Major axis normal to the bonded edge  
\*\*Minor axis normal to the bonded edge